BNL-101419-2014-TECH
AD/PH-23;BNL-101419-2013-IR

GHEISHA Simulation Calculations Of Albedo

A. Gavron

March 1987

Collider Accelerator Department
Brookhaven National Laboratory

U.S. Department of Energy
USDOE Office of Science (SC)

DISCLAIMER

AD/RHIC-PH-23

GHEISHA Simulation Calculations of Albedo

Avigdor Gavron
Los Alamos

3/87

Comparison of Existing and Proposed HEP Data Acquisition Systems and their Suitability for RHIC

Jules W. Sunier
Los Alamos National Laboratory

1. Introduction

A variety of recent topical conferences,[1,2] symposia,[3] and dedicated workshops[4,5] have reviewed the data acquisition (DACQ) existing or proposed for major detectors at High Energy Physics (HEP) collider facilities.

In this note, a summary of these DACQ systems is presented for UA1, MARK II, DO, CDF, and SLD, focussing on the data acquisition stages and trigger rates. The suitability of these systems for a RHIC calorimeter detector with ports is then discussed.

Although these DACQ systems have their individuality, they all use the common approach, illustrated in Fig. 1, of a multi-level trigger that will reduce the rate and volume of the data to be recorded, in a number of appropriate steps. The first level trigger is analog, operates in the 1 μsec range, and has the purpose to reduce the interaction rate to a manageable rate of 10^5 Hz or less. While a second level trigger is being formed, in a time range as short as 10 μsec for SSC detectors, the data can be compressed (zero suppression, pedestal subtraction, etc.) and is buffered. The second level trigger has usually some intelligence, in the form of programmable logic or micro-processors. The third level trigger is done by software. At this stage, it is current practice to employ a processor "farm" to assemble full events and implement the reconstruction necessary to perform the final event selection, prior to archival on tape or optical disc.

The nature and amount of data processing performed at each level is flexible and depends on the application. The differences between the specific systems described below reside in:

- interaction rate and raw event size,
- type of primary data acquisition hardware and read-out scheme,
- choice of busses and processor farms.

The UA1-VME Scheme

Originally using a REMUS-CAMAC parallel read-out scheme, UA1 has now implemented a new VME based read-out system that supports REMUS, FASTBUS and Streamer Tube ADC Readout (STAR), with generalized use of the CPUA1 microprocessor. The event filtering is carried out by a farm of six 168E emulators.

A group of 3081E emulators is planned to perform on-line and off-line analysis. Experiment control is well supported, through VME, by MacIntosh /68000 personal computers.

The data acquisition stages and rates are given in Fig. 2, the timing of trigger levels in Fig. 3. The main bottleneck in the system is the enormous volume of data produced by the Central Drift Chamber, that is reduced and read-out in 25 ms. The first and second level trigger must therefore, without use of the central drift chamber information, reduce the trigger rate to well below 40 Hz.

MARK II for SLC

The DACQ system is shown in Fig. 4. It is a predominantly FASTBUS system, with SLAC Scanner Processors (SSP) used as Segment Interconnect (SI). The overall trigger rate is ~2 Hz with a modest ~40 KBytes per event. A set of on-line 3081E emulators are used to process Flash ADC data, assemble the event and place data in final format to tape. Full "off-line" event reconstruction can be run on-line to monitor detector performance. A SLAC FASTBUS controller (SFC) has been placed in the FASTBUS system crate to supervise the data transfer from the acquisition segments to the processor segment. Another SFC is used to monitor (in parallel with the VAX host) the general instrumentation electronics. SFC application programs are written in FORTRAN, to share code with the more complex VAX monitor programs.

The DO System

A pretrigger (Level-0) initiates data collection at a rate of 50 kHz. To avoid dead-time, the Level-1 trigger must operate within the interval of 3.5 μsec between beam crossings. It uses signals from the calorimeter, an electron tag from the TRD system, and a muon signal from the muon proportional drift-tubes. It passes full events, at the rate of 200-400 Hz, to the second level trigger that consists of a MicroVax II supervisor and 50 parallel analysis nodes, also MicroVax II processors. The level-2 trigger operates, on the average, 100,000 instructions to completely filter one event. It delivers to tape an average event size of 200 KBytes, with a 1-2 Hz rate. The DACQ and online computer system are illustrated in Fig. 5.

The DO DACQ was designed on the basis of two key concepts:

- a single event should be handled entirely by one processor (no splitting or rebuilding should be done)
- use of commercial hardware and software should be maximized.

The read-out section is coupled to the analysis nodes through 8 daisy-chained cables, with an aggregate throughput of 320 MBytes/sec. The input channels feed dual ported memories of 64 KBytes. The data is fed to the node private memory concurrently with the event analysis in progress.

The Host Vax has Ethernet connections to the event processor nodes (running on VAXELN, a software product dedicated to real-time systems) as well as to equipment monitoring computers (more MicroVax II) and μVax workstations. It is interesting to note that the off-line processing needs of DO are estimated to be 50 to 100 VAX 780 years. The on-line system has 50 VAX 780 equivalents.

The CDF System

The primary trigger rate is 50 kHz and a typical event size is 100 KBytes. Three levels of triggering pass events for recording at a rate of 1–5 Hz. The Level-1 trigger, deadtime less, operates on mostly calorimetric information and reduces the trigger rate to 5 kHz. The Level-2 trigger uses the same information as Level-1, with more sophistication. It takes from 20–100 μsec and reduces the trigger rate to ~100 Hz. Intelligent Readout Scanners perform the digitization in 1–4 μsec, each scanner having storage space for 4 events. The system is shown in Fig. 6.

A Buffer Manager (μVax II) directs the Event Builder that is responsible for the accumulation of all data from the scanners. Two trigger supervisors are used to allow calibration and diagnostics to run concurrently with the data taking.

The Level-3 trigger, a multiprocessor system with a processing power of ~10 VAX 11/780, reduces the event rate from 100 Hz to 1–10 Hz to be available for consumer processes on the VAX online computers. Each of these computers (1 primary VAX 11/785 Host, 3 secondary VAX 11/750 for monitoring and control, 1 alarm monitoring VAX 11/730 with serial CAMAC) is connected to FASTBUS through a UNIBUS processor interface, allowing each of them simultaneous access to the events in the Level-3 farm.

The CDF DACQ system runs on the concept of independent multiple partitions, sections of the detector that function independently of other sections. Each partition has its own read-out scanners and can receive independent triggers. The buffer manager and event builder operate on all partitions, with appropriate readout lists. This concept is very powerful for parallel debugging or calibration. The partitions are dynamic, down to the basic unit of a single readout scanner.

The SLD System

The low 180 Hz repetition rate of SLC allows for a very "simple" software trigger (5.5 msec between crossings), performed by SSP's processing coded hit information from the drift chambers and the energy sums of the liquid argon calorimeter, which are fully digitized in ~1 msec. Triggered events are fully digitized in ~50 msec and buffered into the SSP memory of each FASTBUS crate, as indicated in Fig. 7. Further processing (~200–400 msec) is done by the SSP's, prior to passing full events to a μVaX processor farm, at the trigger level of 1–2 Hz. Finally, events are logged and sampled by the host computer. A typical event size of 100 KBytes is obtained from 96 MBytes of digitized data.

Suitability of Described Systems for RHIC

According to the proceedings of the Workshop on Experiments for RHIC,[6] the major components of a calorimeter, with a slit spectrometer for the central region, are:

a. ~2300 Electromagnetic and Hadronic cells in the central part of the calorimeter, 800 Electromagnetic and 200 Hadronic cells in each of the end caps, or a total of ~6600 channels of data.

b. A multiplicity detector (DC with pad-read outs, silicon pads, streamer tubes?) with about 10^5 cells.

c. A port equipped with an inside TPC (10^4 channels), a RICH detector (5×10^3), external tracking chambers (10^3) and TOF counters (225).

In addition, one has to provide a Vertex Detector, due to the extent of the interaction region. This detector could easily have 10^5–10^6 channels.

The above very approximate numbers lead to a final event size of the order of 100 KBytes, while the uncompressed event could be of the order of several megabytes. The following table summarizes the trigger and event rates, as well as the taped event size of the detectors described in this note. One can easily see that the RHIC calorimeter under study will have DACQ requirements quite similar to those of UA-1, DO and CDF. While the hardware/software choices can only be made when the detector has been designed, it is clear that much can be learned from the above mentioned HEP detectors. It should also be clear that the DACQ of the detector will be a significant part of its design effort and cost, and that work along that line should be started at the earliest feasible stage.

References

1. Fourth Conference on Real Time Computer Applications in Nuclear and Particle Physics, Chicago, May 20-24, 1985. IEEE Transactions on Nuclear Science, Volume NS-32, No. 4, August 1985.

2. VME bus in Physics Conference, CERN, Geneva, Oct. 7-8, 1985. CERN 86-01, January 1986.

3. 1985 Nuclear Science Symposium, San Francisco, October 23–25, 1985. IEEE Transactions on Nuclear Science, Volume NS-33, No. 1, Feb. 1986 (see also 1983, 1984, 1986 NS Symposia).

4. Proceedings of the FNAL Workshop on Triggering, Data Acquisition and Computing for High Energy/High Luminosity Hadron-Hadron Colliders (March 1986).

5. Report of the Task Fore on Detector R&D for the SSC, June 1986.

6. RHIC Workshop: Experiments for a Relativistic Heavy Ion Collider, BNL, August 15–19, 1985. Report BNL 51921.

TABLE I

Event Rates, Trigger Rates and Recorded Event Size for Various HEP Detectors Compared to a RHIC Calorimeter with Slit Spectrometer

Detector	Pre-Trigger Rate	Level-1 Trigger	Level-2 Trigger	Level-3 Trigger	Event Size
UA-1	1.5×10^5	100	20	5	120 kb
MARK II	2×10^2			2	40 kb
D0	5×10^4	2–400		1–2	200 kb
CDF	5×10^4	5000	100	1–10	$\sim$ 100 kb
SLD	2×10^2			1–2	100 kb
RHIC CALO/SLIT	$10^4 - 10^5$			$\sim$ 5	$\sim$ 100 kb

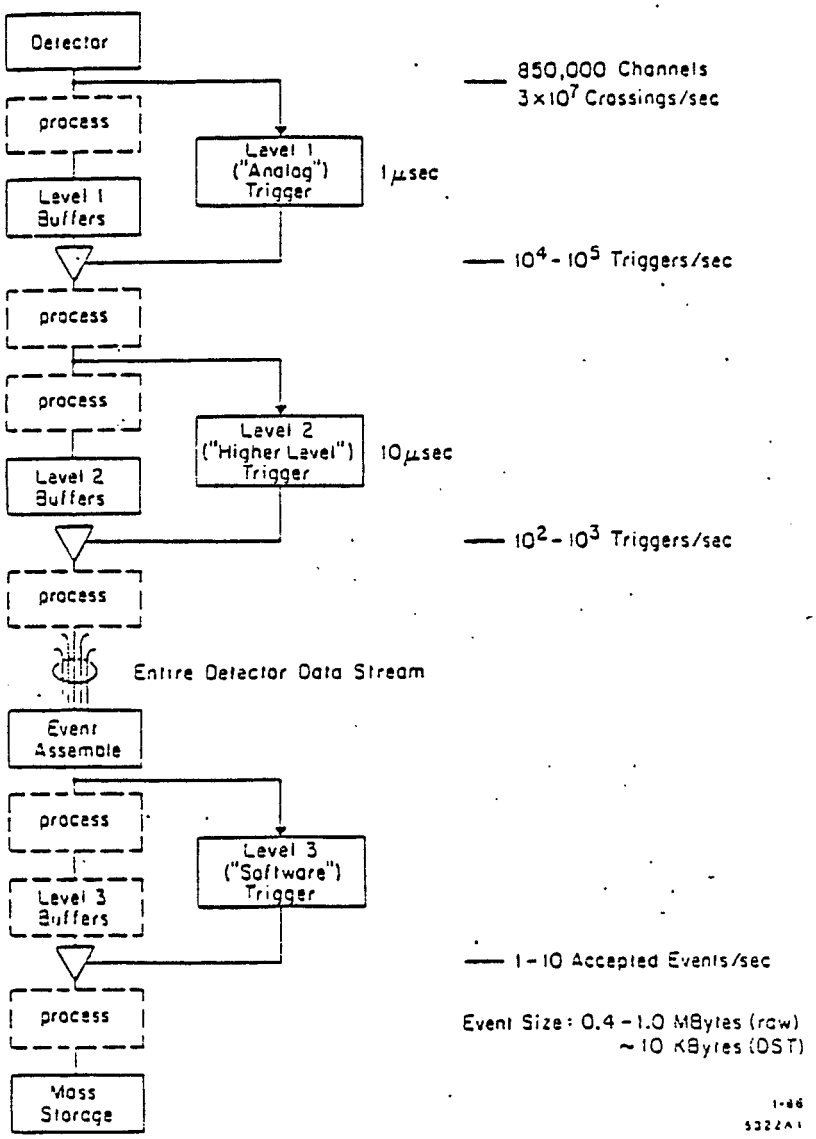

Fig. 1 General model of data flow through levels of the data acquisition.

(A.J. Lankford and G.P. Dubois, Ref 4)

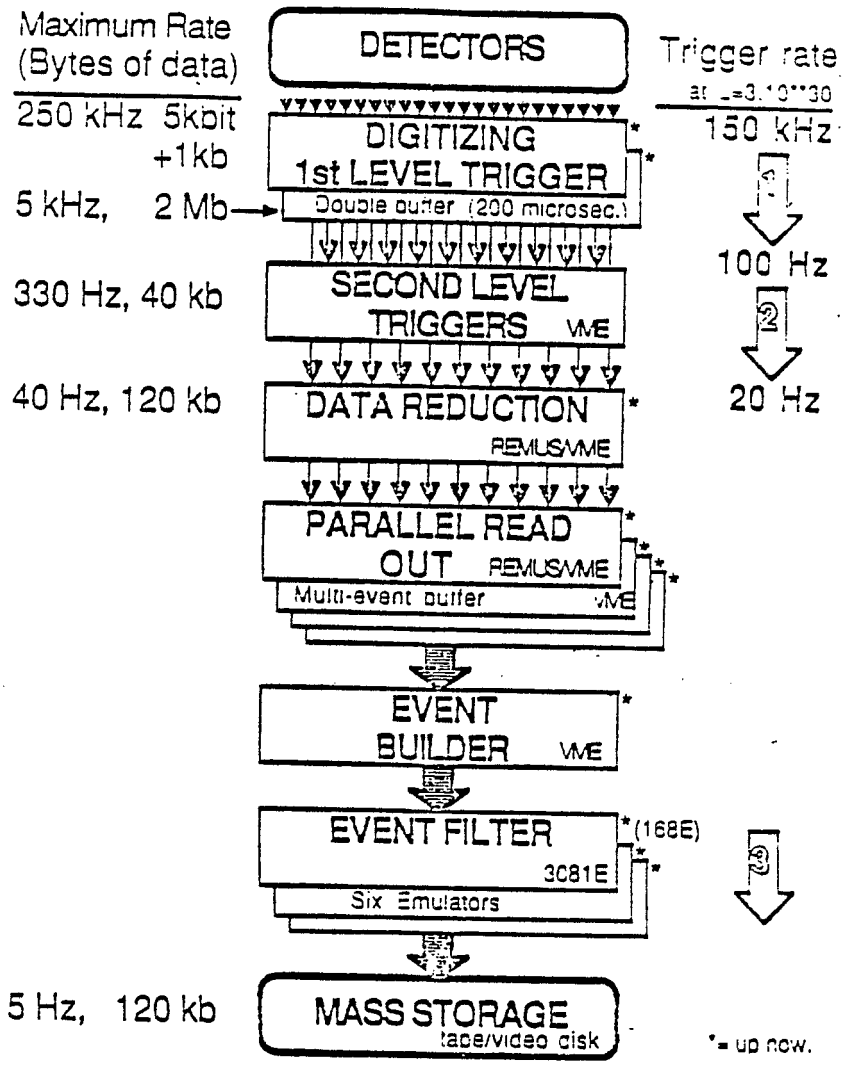

Figure 2. Overview of UA1 trigger levels and data acquisition. At the left the maximum possible rates of the different levels are indicated. The right column gives the target rates for the trigger. The dead time will be <10 %

(S. Cittolin, Ref. 2)

Fig. 3. TIMING OF TRIGGER LEVELS - UA1

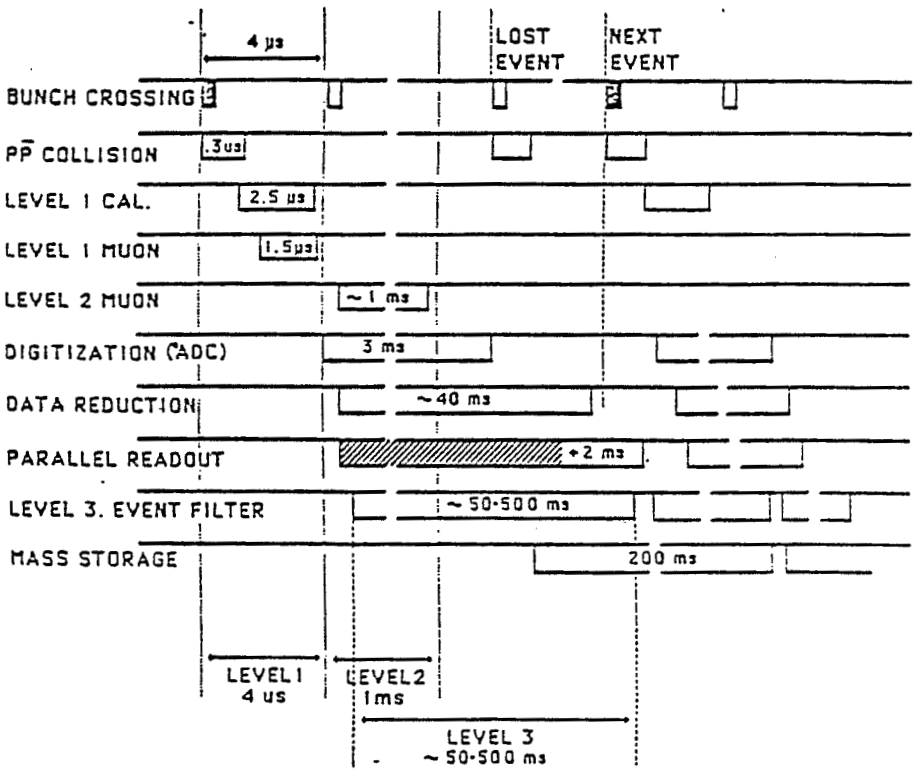

(S. Cittolin, Ref. 2)

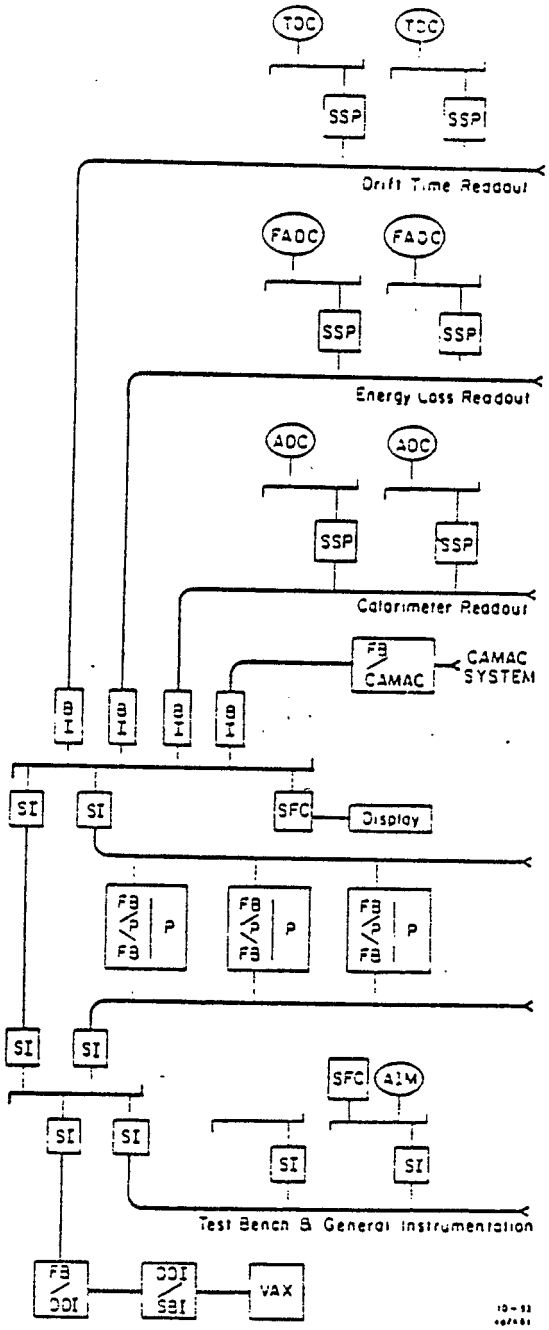

Fig. 4. Fastbus architecture for MARK II

A.J. Lankford and T. Glanzman,
IEEE Transactions NS-31, No. 1 (1984)

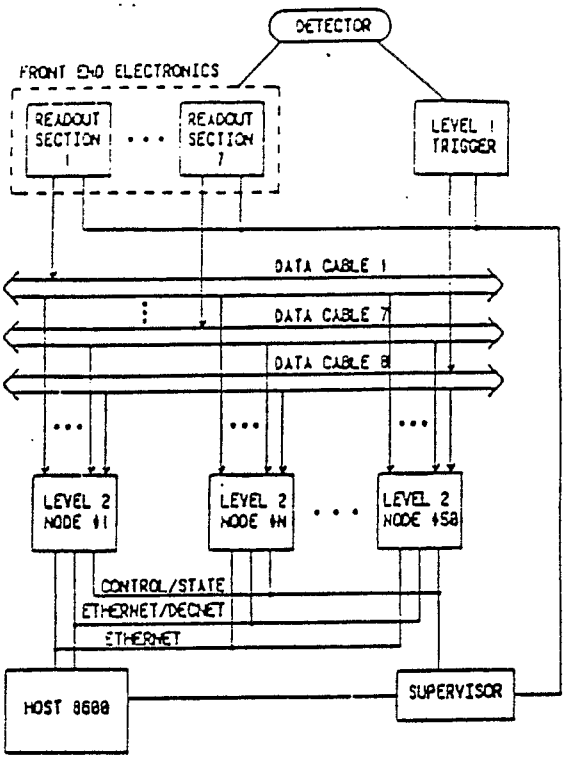

a) Block diagram of acquisition system.

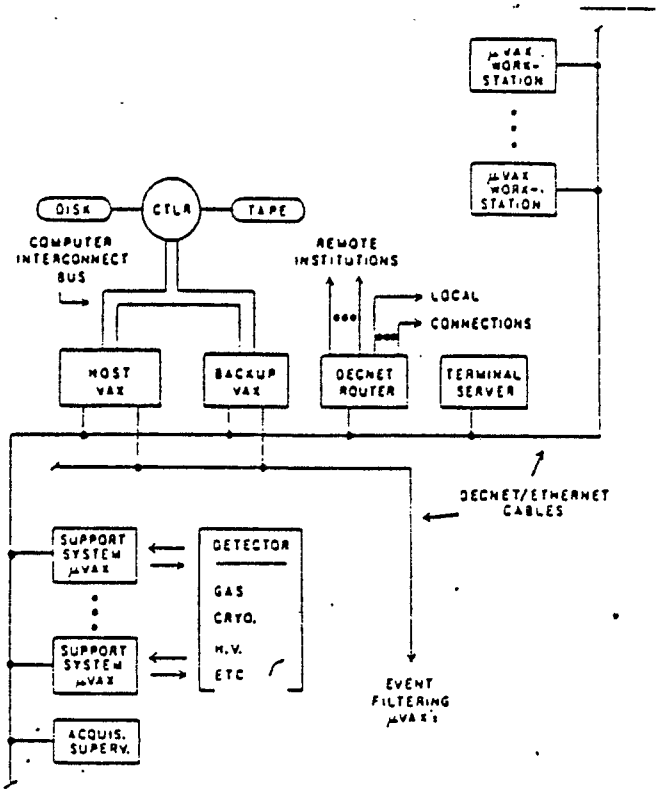

b) Online computer system.

Fig 5. DO Data Acquisition Design
(D. Cutts et. al, Ref. 1)

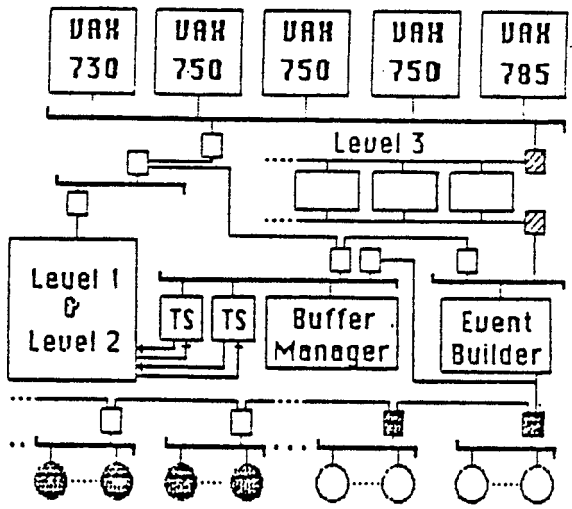

CDF Data Acquisition Hardware

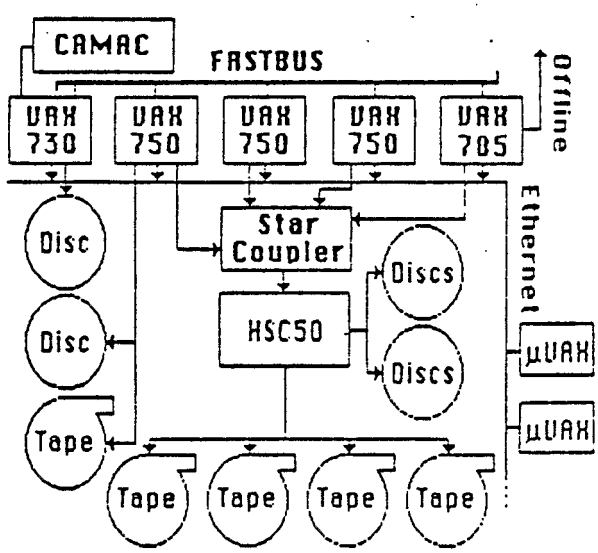

CDF Online Computer Configuration

Fig. 6: CDF Data Acquisition Design

(D. Quarrie, Ref. 1)

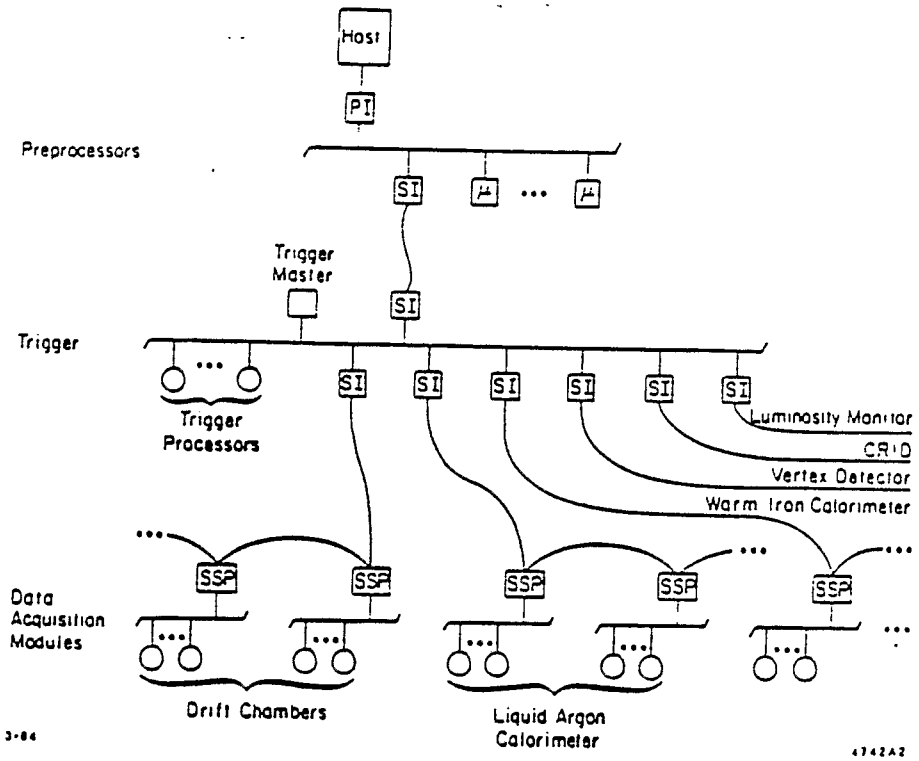

SLD. FASTBUS configuration.

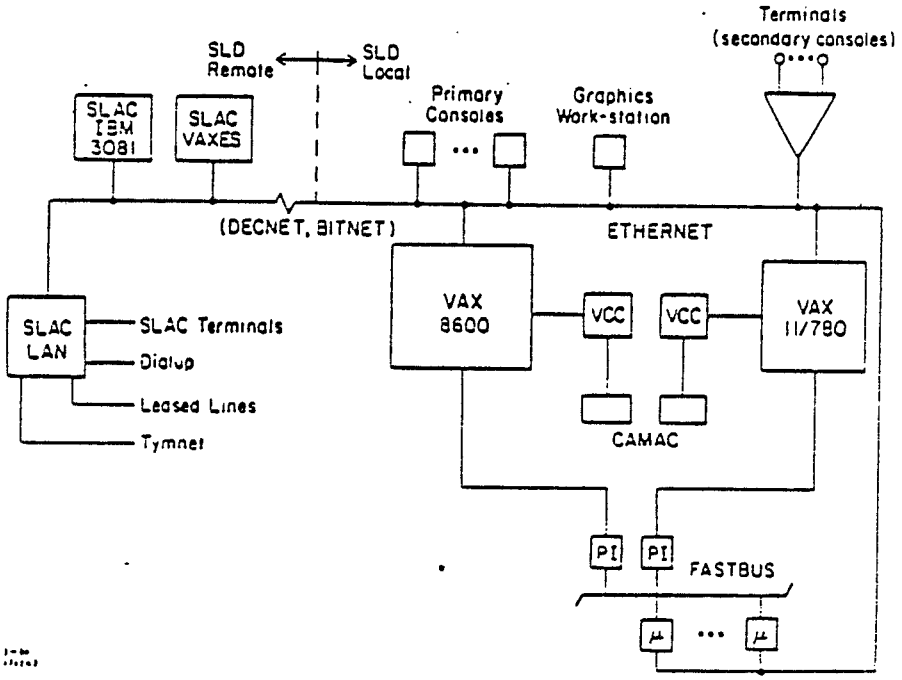

SLD. Host computer configuration.

Fig. 7. SLD Data Acquisition Design
(D.J. Sherden, Ref. 1
R.S. Larsen, Ref. 3)

GHEISHA simulation calculations of albedo

Avigdor Gavron, Los Alamos

Introduction

The pupose of this note is to present some results of albedo calculations using the code GHEISHA version 6, of H. Fesefeldt, Aachen, FRG. Until confronted with experimental results, these results should be used to obtain order of magnitude of albedo effects only. Their purpose is to enable designers of detectors for RHIC and other facilities to estimate the effect of albedo from a Uranium/Scintillator calorimeter on other detectors. The calorimeter used in the simulation is comprised of alternating Uranium plates (3 mm. thick) and scintillator plates (also 3 mm. thick). The total depth of the calorimeter is 6.4λ. The plates were cirular with a radius of 1 meter. The beams (p,n,π-s) impinged perpendicular to the plates at the center of the circle.

Results

We have performed calculations for beam kinetic energies of 0.2, 0.5, 2, 5, 20 and 50 GeV. For each of these energies we present detailed results for $dE/d\Omega$ and $dN/d\Omega$ (the total kinetic energy and particle multiplicity per unit solid angle) for albedo neutrons. There is a threshold of 5MeV, below which albedo neutrons are discarded. (This is due to lack of disk space for the albedo file generated by GHEISHA but should not affect the conclusions). For albedo pions and protons, the albedo results are less accurate due to the very limited statistics of the Monte-Carlo simulation. The results were obtained using 2 weeks of CPU-time on a microvax II computer(!), so it was not

feasible to obtain significantly better statistics. Thus, I can only summarize the average albedo-pion kinetic energy:~100MeV; the albedo-pion multiplicity is presented in Fig. 9. The proton-albedo multiplicity is somewhat lower and consequently - the statistics too poor to present any meaningful result. The few proton events seem to indicate that the proton kinetic energy is of the order of 50-200 MeV.

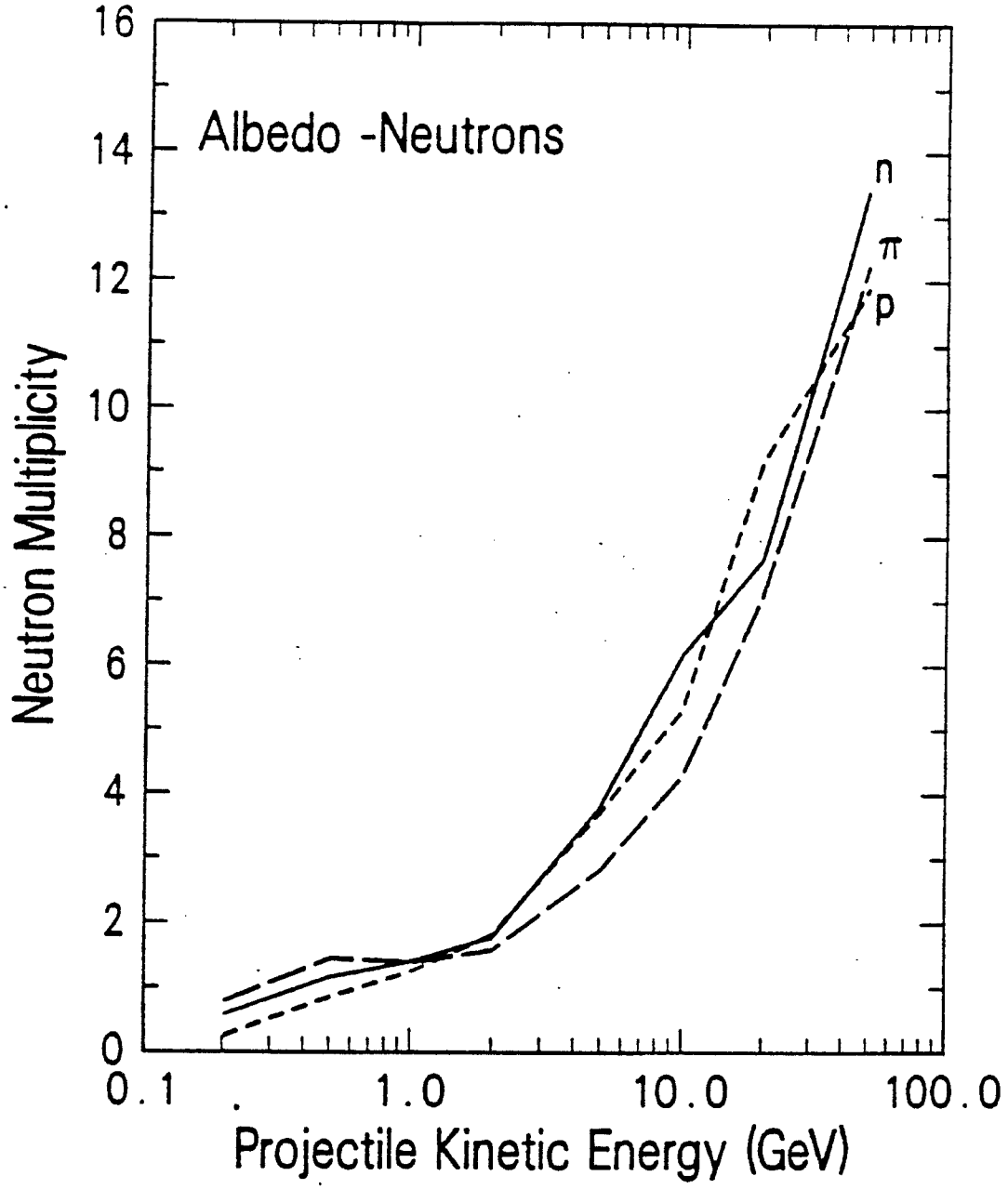

Fig. 1: Albedo neutron multiplicity as function of projectile kinetic energy. The curves are labelled by the projectile.

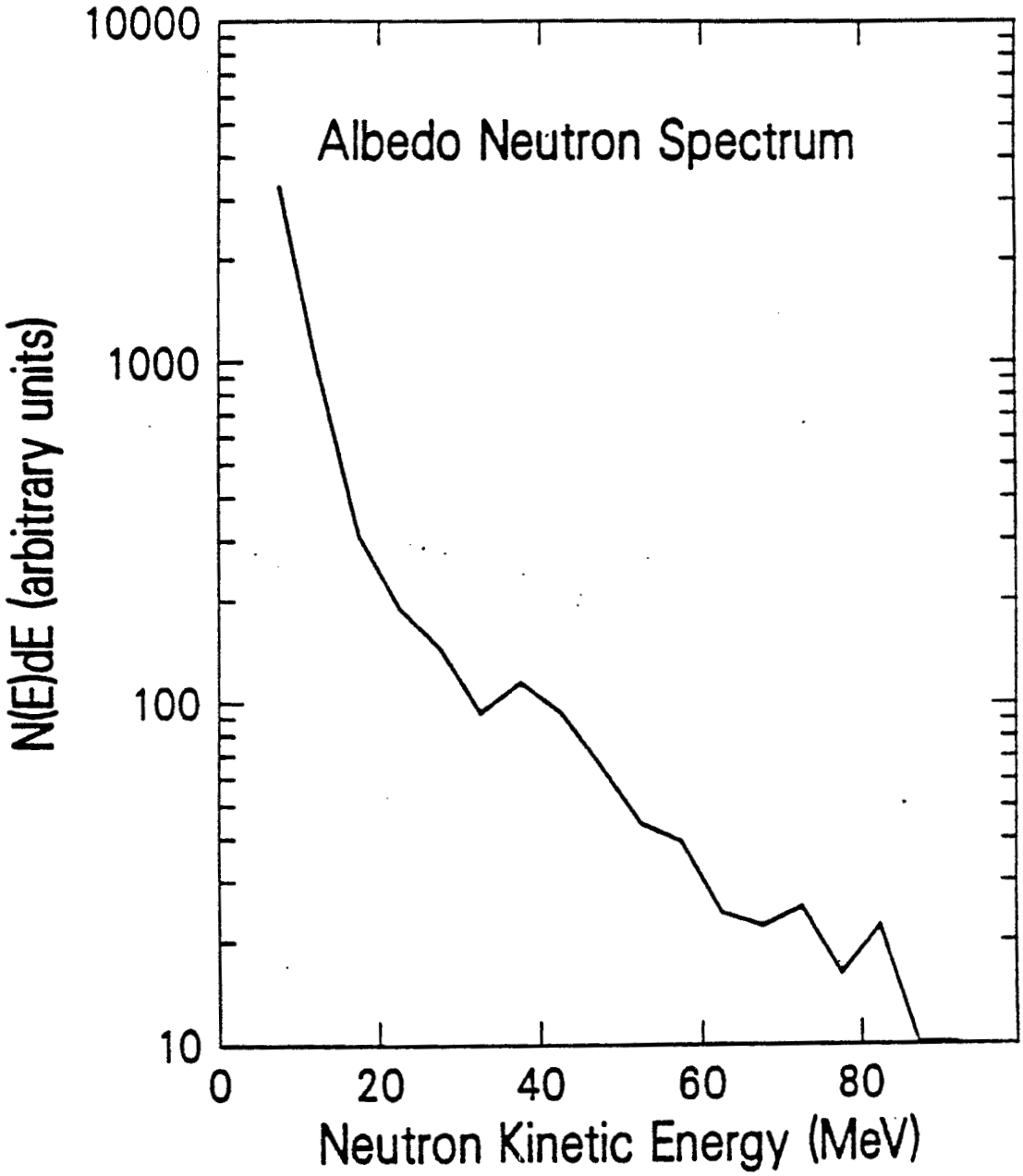

Fig. 2: Albedo neutron spectrum for 5 GeV pions. There is no significant variation between neutron spectra produced by other projectiles at other bombarding energies.

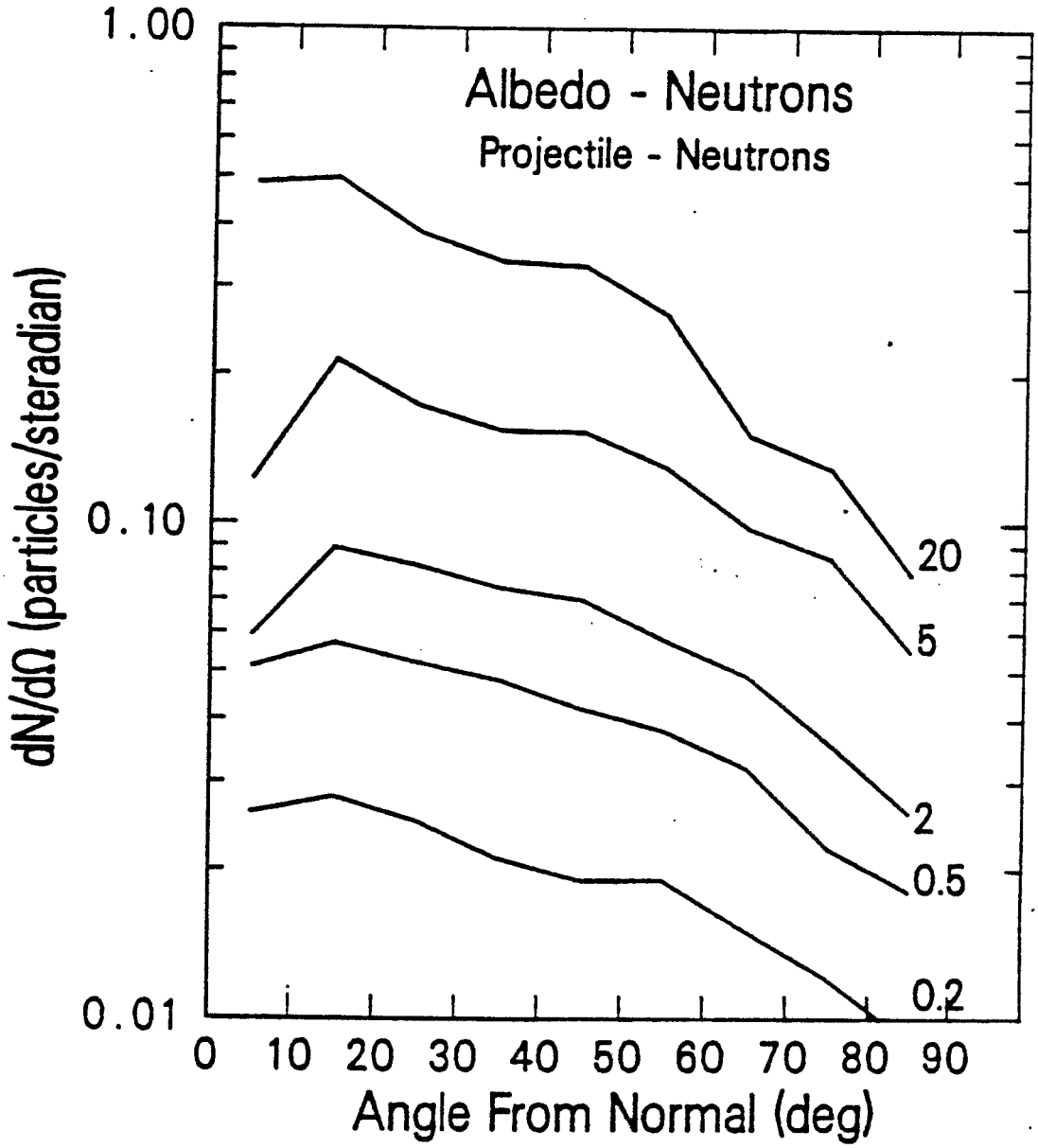

Fig. 3: Albedo neutron angular distribution. Projectile - neutrons. Curves are labelled by the projectile kinetic energy.

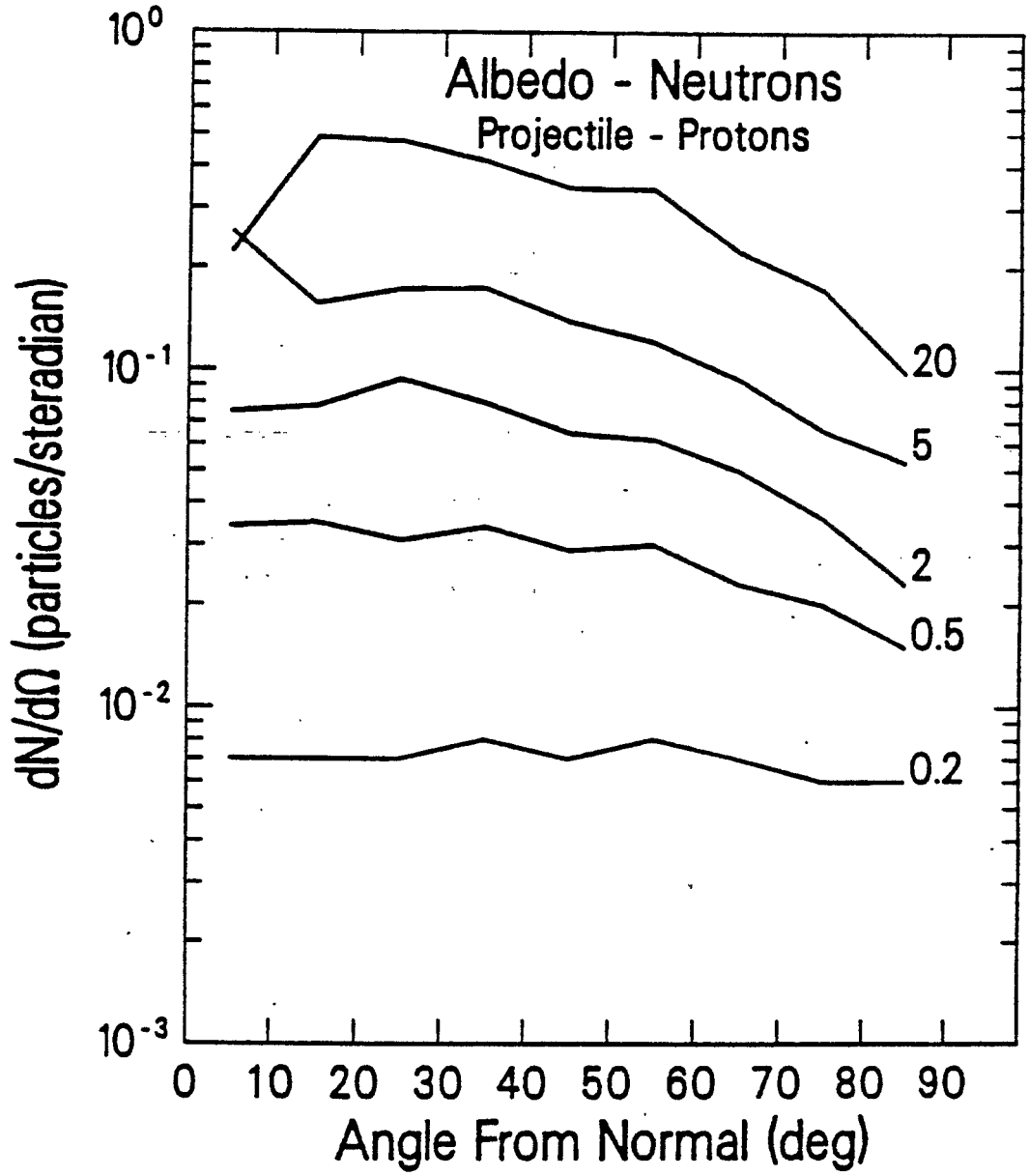

Fig. 4: Albedo neutron angular distribution. Projectile - protons. Curves are labelled by the projectile kinetic energy.

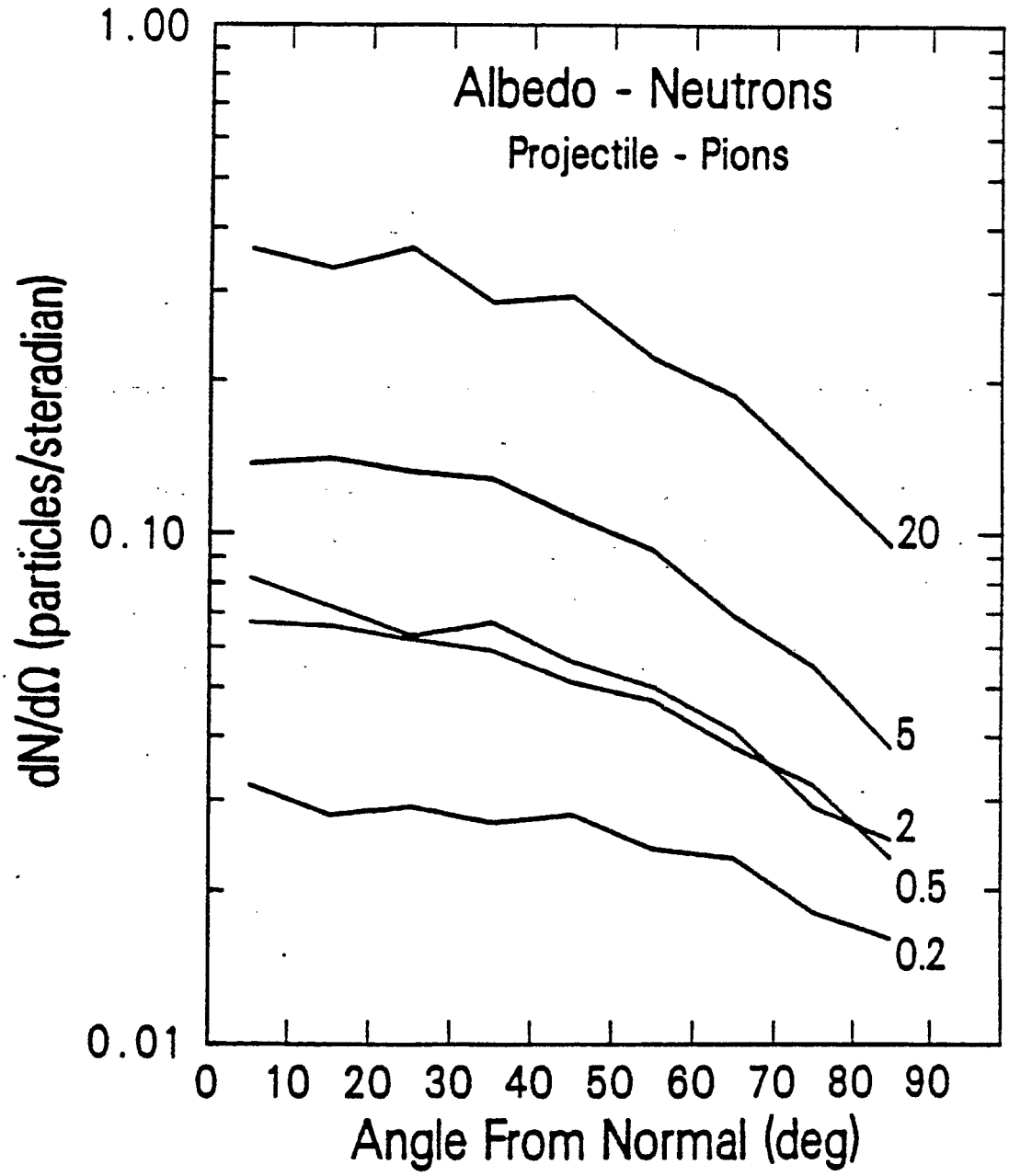

Fig. 5: Albedo neutron angular distribution. Projectile - pions. Curves are labelled by the projectile kinetic energy.

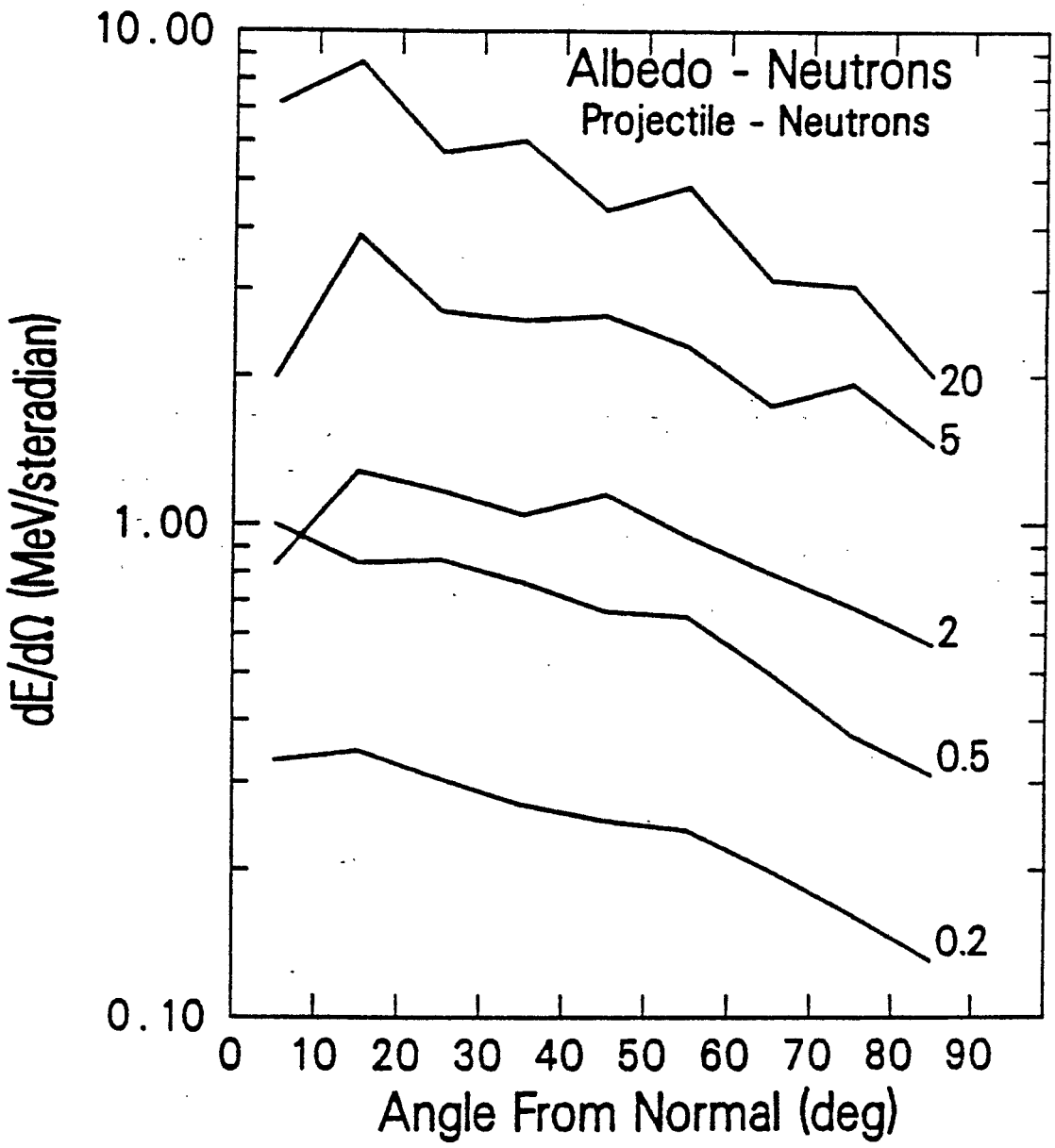

Fig. 6: Albedo neutron energy per unit solid angle. Projectile - neutrons. Curves are labelled by the projectile kinetic energy.

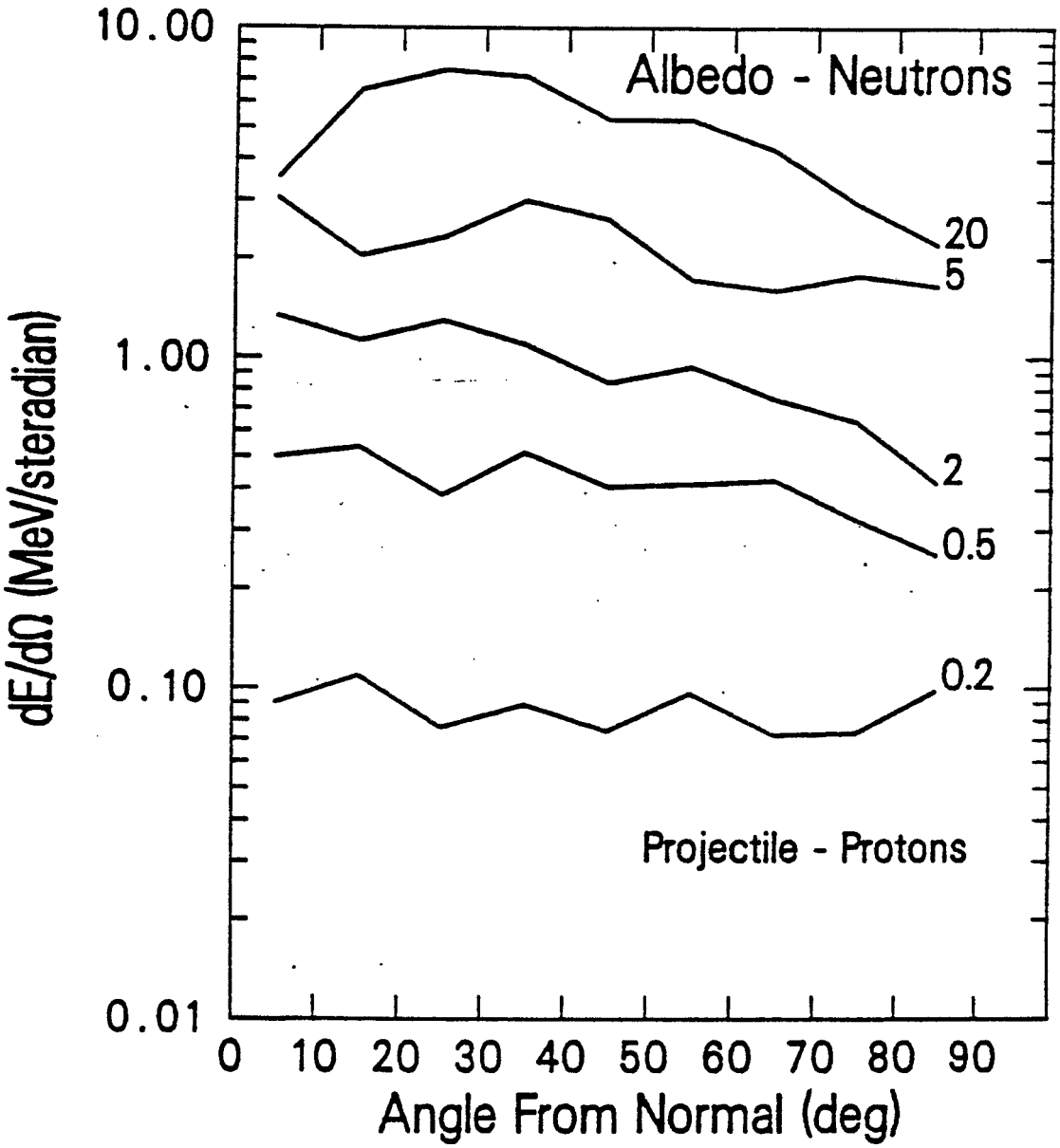

Fig. 7: Albedo neutron energy per unit solid angle. Projectile - protons. Curves are labelled by the projectile kinetic energy.

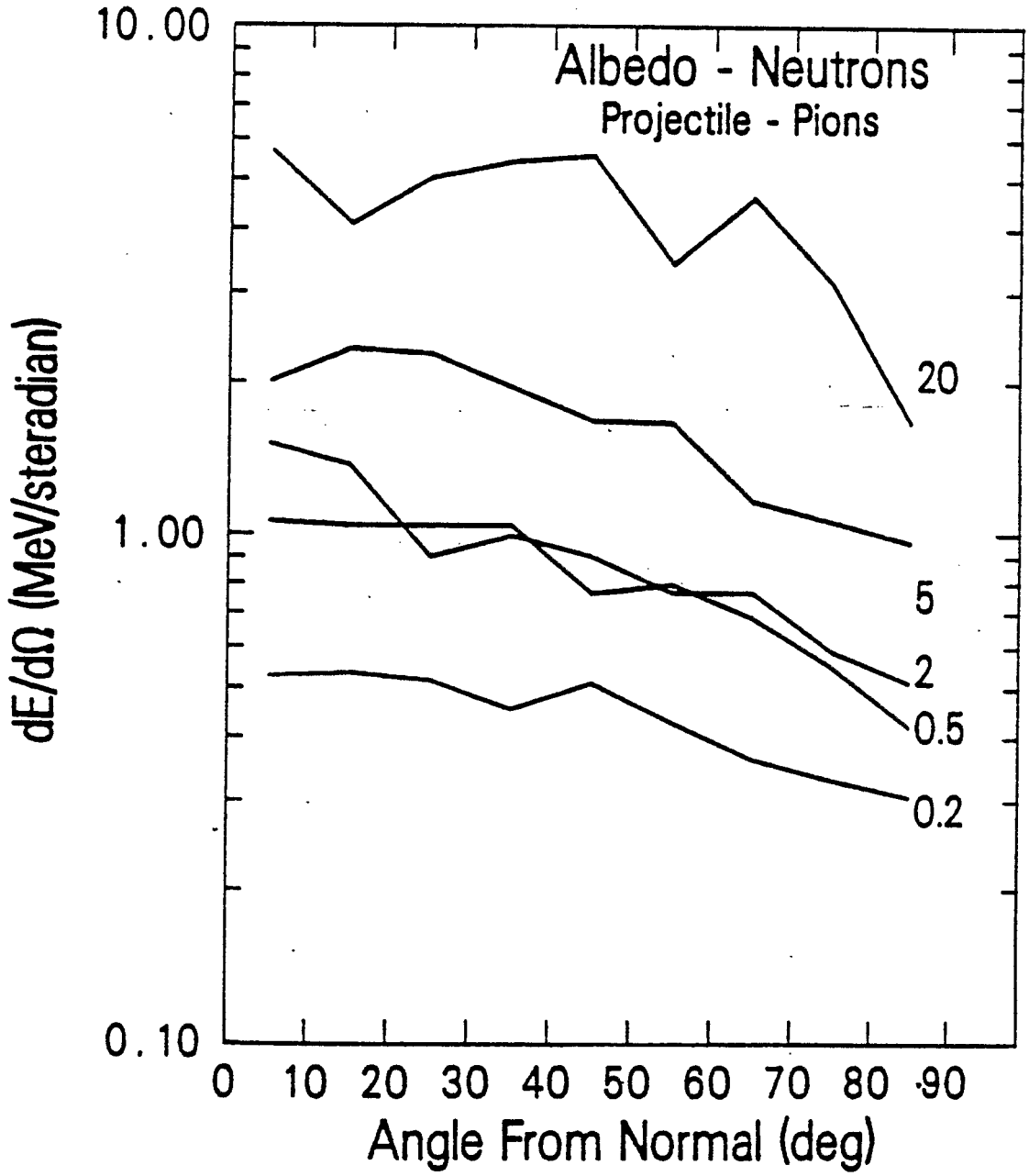

Fig. 8: Albedo neutron energy per unit solid angle. Projectile - pions. Curves are labelled by the projectile kinetic energy.

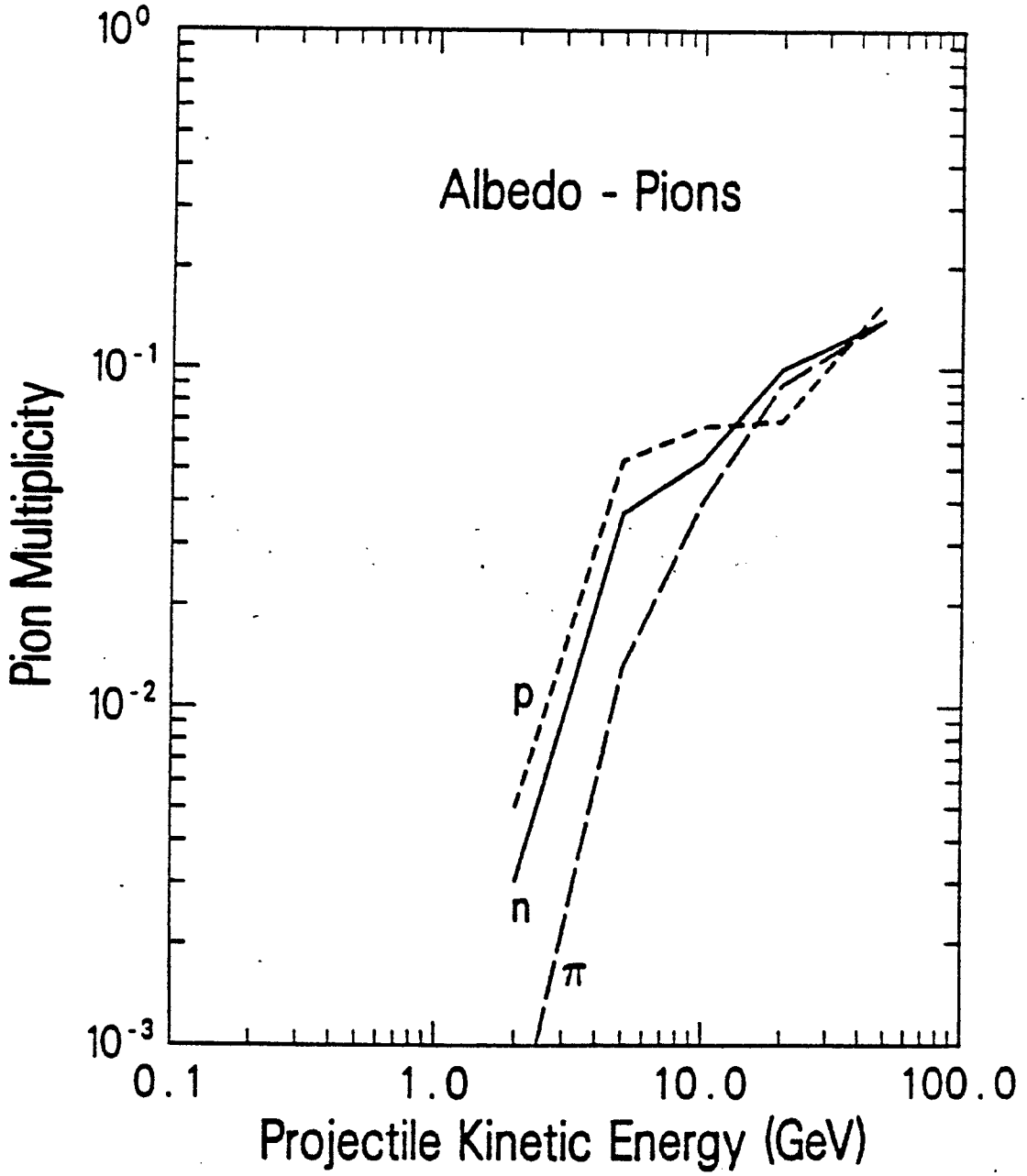

Fig. 9: Albedo pion multiplicity as function of projectile kinetic energy. Curves are labelled by type of projectile particle.